Optica Applicata, Vol. XLII, No. 3, 2012
DOI: 10.5277/oa120308

Presence of spherical aberration in the reference as a possible source of variations in magnitude of measured ocular aberrations

VARIS KARITANS[1, 2*], MARIS OZOLINSH[1, 2], KAIVA LUSE[2], LASMA EKIMANE[2]

[1]Institute of Solid State Physics, University of Latvia,
8 Kengaraga Street, LV-1063, Riga, Latvia

[2]Department of Optometry and Vision Science, University of Latvia,
8 Kengaraga Street, LV-1063, Riga, Latvia

[*]Corresponding author: variskaritans@gmail.com

Different aberrometry methods exist and the magnitude of measured wavefront aberrations may differ depending on the method used. Even several Shack–Hartmann wavefront sensors may demonstrate clinically significant differences between ocular aberrations measured. In this study, we tested a hypothesis that a possible source of systematic error in Shack–Hartmann aberrometry may be the presence of spherical aberration in the wavefront used for calibrating the Shack–Hartmann wavefront sensor. Six subjects participated in the study. The Shack–Hartmann wavefront sensor was calibrated by using a spherical and an aspheric lens. Statistically significant changes in wavefront aberrations were observed when comparing both references. Clinically significant changes in magnitude of spherical aberration were also observed. We conclude that for precise measurement of aberrations the use of an aspheric lens for wavefront sensor calibration is essential and different sphericity of the wavefront used for calibration purposes may give rise to variability between wavefront data measured by different Shack–Hartmann wavefront sensors.

Keywords: wavefront, ocular aberrations, adaptive optics.

1. Introduction

The human eye is not a perfect optical system and suffers from various kinds of aberrations [1–3]. Aberrations both affect visual perception and reduce the resolution in retinal images. Aberrations are divided into two broad classes: lower-order aberrations (LOA) and higher-order aberrations (HOA). Since adaptive optics have been used by vision scientists there has been steadily growing interest in the role of HOA in improving visual functions and increasing resolution in retinal images [4].

Two main elements of adaptive optics systems are Shack–Hartmann wavefront sensor (SHWS) and a wavefront modulator. Principles of the SHWS can be found in many literature sources [5, 6]. Shortly, the incoming wavefront is sampled by a lenslet array placed in front of a charge-coupled device (CCD). If a plane wavefront is incident on the lenslet array an absolutely symmetric grid of spots is created on the CCD sensor, each spot being located on the optical axis of the corresponding lenslet. If the wavefront is distorted, the spots deviate away from positions in which they are located in the case of a plane wavefront. The wavefront is reconstructed by measuring the distance by which the light spots have deviated.

Measurement and correction of wavefront aberrations requires a reference against which these aberrations are measured and which is to be achieved by wavefront correction. As mentioned previously any incoming wavefront is compared to a plane wavefront by measuring spot deviations, *i.e.*, the reference is the plane wavefront. The software we use requires that a plane wavefront be defined and it must be defined by a bitmap file containing information about location of spots. Further in the text, the bitmap file containing information about location of the spots will be what we will refer to as a reference. Theoretically, the ideal reference is defined by a bitmap file in which spots are organized absolutely symmetrically. However, because of imperfections in manufacturing process the pitch of the lenslet array is not constant and absolutely symmetric grid of the spots is not the optimal reference. Thus the ideal reference is one which is obtained by letting a perfectly plane wavefront enter the SHWS.

Unfortunately, there is almost no literature available regarding the way the reference is set. For calibrating the SHWS, CHERNYSHOV *et al.* [7] used a spherical wavefront emerging from one end of a single-mode polarization maintaining fibre. The use of the fibre helped to avoid aberrations in the emerging spherical wavefront almost completely. After propagating several meters its curvature is small and a reference close to the ideal one is obtained. Similarly to CHERNYSHOV *et al.*, ARTZNER [8] used for calibrating purposes either a spherical wavefront with a large radius of curvature or a parallel beam formed by the central region of a converging lens.

The calibration of the SHWS and the choice of the reference may affect magnitude of the measured wavefront aberrations. In vision science, knowledge of exact values of Zernike coefficients is necessary when characterizing optical performance of intraocular lenses, evaluating success of refractive surgery, investigating distribution of Zernike coefficients in a population, measuring the wavefront aberrations for adaptive optics correction, *etc*. It is known that magnitude of the measured aberrations differs when using different aberrometry methods such as Shack–Hartmann, Tscherning, ray-tracing, skiascopy, Placido discs, keratography and others [9]. Despite the considerable number of aberrometry methods, the Shack–Hartmann aberrometry is the most popular one used both in astronomy and in vision science. However, even different SHWS do not provide unequivocal wavefront data [10] and even the wavefront sensing principle behind all these SHWS is one and the same. The aim of this study was to assess the systematic error of wavefront measurements caused by

differences in the reference spot pattern because of spherical aberration in the reference wavefront.

2. Methods

2.1. Subjects

Six subjects (VK, GK, KL, JS, LE, and MD) were enrolled in the experiment. Only aberrations of the right eyes were measured. Subjects JS and MD had a moderate degree of myopia while subject GK had high level of myopia. Subject VK had small myopic refractive error. The other two subjects LE and KL had small degree of hypermetropia. Refraction of the subjects is summarized in Table 1.

T a b l e 1. Refractive errors in subjects participating in the study.

Subject	Sphere	Cylinder
VK	–0.50 D	–0.50 D
GK	–5.00 D	–0.75 D
KL	+0.50 D	0.00 D
JS	–3.75 D	0.00 D
LE	+0.50 D	+0.25 D
MD	–2.00 D	–1.50 D

None of the subjects reported any previous or present ocular pathology or injury. All the subjects were introduced to the aim of the study and agreed to take part in the experiment.

2.2. Calibration of the SHWS

We designed our optical layout similar to that used by ARTZNER [8]. The optical layout for setting the reference is shown in Fig. 1. A laser beam (wavelength $\lambda = 670$ nm emitted by a solid state RGB laser) was focused onto one end of a single-mode polarization maintaining fibre by means of a spherical lens L1. The outgoing beam

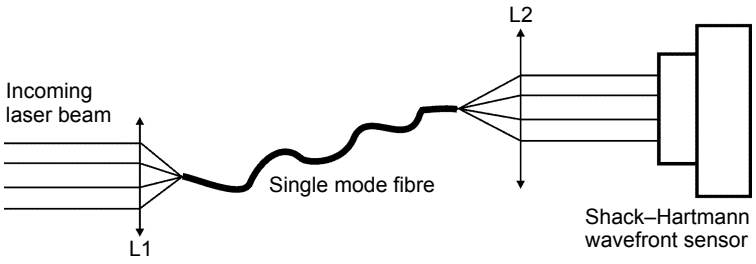

Fig. 1. The optical layout for setting the reference. A laser beam is focused on one end of a single-mode polarization-maintaining fibre by means of lens L1, while the other end is placed at the first focal point of a collimating lens L2 that can be either spherical or aspheric. The SHWS is placed behind lens L2.

was collimated by placing the other end of the fibre in the first focal plane of a converging lens L2 that was either a spherical lens (f = 180 mm) or an aspheric ophthalmic lens (f = 200 mm). The reference created by the aspheric lens will be called an aspheric reference. In the case of a spherical lens it will be called a spherical reference. In case the lens L2 was spherical the end of the fibre was placed in the focal plane of the paraxial region. The use of the fibre helped to avoid aberrations in the spherical wavefront before the lens and homogenized the beam. The collimation degree of the beam was controlled by comparing the beam diameters close to the lens L2 and at a distance of several meters away from the lens.

A centroiding algorithm [11] was applied to the grid of the spots to locate the centroids:

$$x_c = \frac{\sum_{i=1}^{U}\sum_{j=1}^{V}\left[I(i,j) - I_n\right]}{\sum_{i=1}^{U}\sum_{j=1}^{V}\left[I(i,j) - I_n\right]H(i,j)} H(i,j)x_{i,j}$$

$$y_c = \frac{\sum_{i=1}^{U}\sum_{j=1}^{V}\left[I(i,j) - I_n\right]}{\sum_{i=1}^{U}\sum_{j=1}^{V}\left[I(i,j) - I_n\right]H(i,j)} H(i,j)y_{i,j} \tag{1}$$

Indices i and j identify the location of the pixel within a subaperture. The parameters x_{ij} and y_{ij} are the coordinates of the pixel (with indices i and j within a subaperture) in the whole grid of the spots. $I(i,j)$ is the intensity of the pixel with indices i and j. I_n is intensity of the n-th intense pixel within the subaperture. $H(i,j)$ is a binary parameter and can take only values 1 or 0:

$$H(i,j) = \begin{cases} 1 & \text{if} \quad \left[I(i,j) - I^n\right] \geq 0 \\ 0 & \text{if} \quad \left[I(i,j) - I^n\right] < 0 \end{cases} \tag{2}$$

2.3. Measuring aberrations

Measurement of the aberrations was divided into two stages. In the first stage, ocular aberrations summed with the aberrations of the optical system inherent to it. They were measured by using the standard optical layout shown in Fig. 2. For measuring the sum of ocular aberrations and aberrations inherent to the optical system an infrared laser beam at λ = 850 nm was focused on the retina. The power P = 100 μW at the corneal level. Prior to entering the eye the beam was divided by a 50/50 pellicle beam splitter

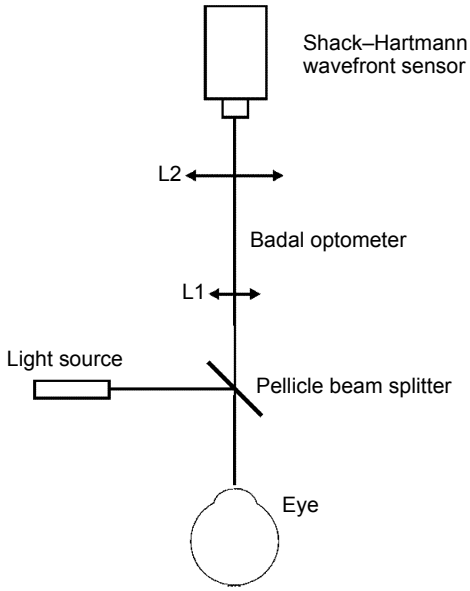

Fig. 2. The optical layout for measuring ocular aberrations. The light source was an infrared laser. The outgoing wavefront was expanded by the Badal optometer used to correct defocus of the optical system. The ocular aberrations were measured by the SHWS – see the text for details.

(Thorlabs). The Badal system consisting of two lenses L1 and L2 was used to expand the pupil of the eye to the size of the entrance pupil of the SHWS. The lenses L1 and L2 were placed so that at $\lambda = 670$ nm defocus was 0 D when measured against the aspheric reference. The focal length of the lenses L1 and L2 was 45 mm and 200 mm, respectively. Next, the beam was directed into the SHWS. We used an SHWS model SHAH-0620A (Visionica) for measuring ocular aberrations. The magnitude of tip and tilt was minimized by using fine adjustment screws of the SHWS. Ocular aberrations were measured in cycloplegia. The pupil was dilated by a 1% cyclogil solution. There was a few minutes' interval between two consecutive measurements.

The measured wavefront aberrations were converted to objective refraction data by using equations found in [12]:

$$M = \frac{-c_2^0 4\sqrt{3} + c_4^0 12\sqrt{5} - c_6^0 24\sqrt{7}}{r^2}$$

$$J_0 = \frac{-c_2^2 2\sqrt{6} + c_4^2 6\sqrt{10} - c_6^2 12\sqrt{14}}{r^2} \tag{3}$$

$$J_{45} = \frac{-c_2^{-2} 2\sqrt{6} + c_4^{-2} 6\sqrt{10} - c_6^{-2} 12\sqrt{14}}{r^2}$$

In the next stage, the aberrations of the optical system were measured and subtracted from aberrations measured in the first stage to obtain the ocular wavefront data. Zernike coefficients can be linearly summed within the unit circle. The aberrations of the optical system were measured at the wavelength $\lambda = 670$ nm by placing a plane mirror in the position of the eye. We did not expect a significant measurement error to result from using two different wavelengths 670 nm and 850 nm for measuring aberrations. Each measurement was repeated 5 times. The average value and standard error for each Zernike coefficient was calculated from all measurements. As previously, there was a few minutes' interval between two consecutive measurements.

3. Results

3.1. Analysis of spot patterns

First, we analyze the Shack–Hartmann spot positions. The deviations of the centroids in the central and the peripheral regions of the pixel array are shown in Fig. 3. The red columns correspond to the reference set with the aspheric lens, while the green columns are shown for the spherical case. If the aspheric lens is used for setting the reference a plane wavefront is incident on the lenslet array and the pitch of the pixel array (in μm) can be calculated by dividing the lenslet pitch (150 μm) by the average distance of two neighbouring centroids expressed in pixels (12.77 pixels), *i.e.*, the pixel pitch $P = 11.75$ μm. To estimate the reliability of this calculation the pixel pitch is multiplied by the size of the array, *i.e.*, $(N-1)P = 6$ mm where N is the number of pixels along one dimension. This value coincides well with the size of the exit pupil of the SHWS. We also calculated the dynamic range of the SHWS. The dynamic range can be

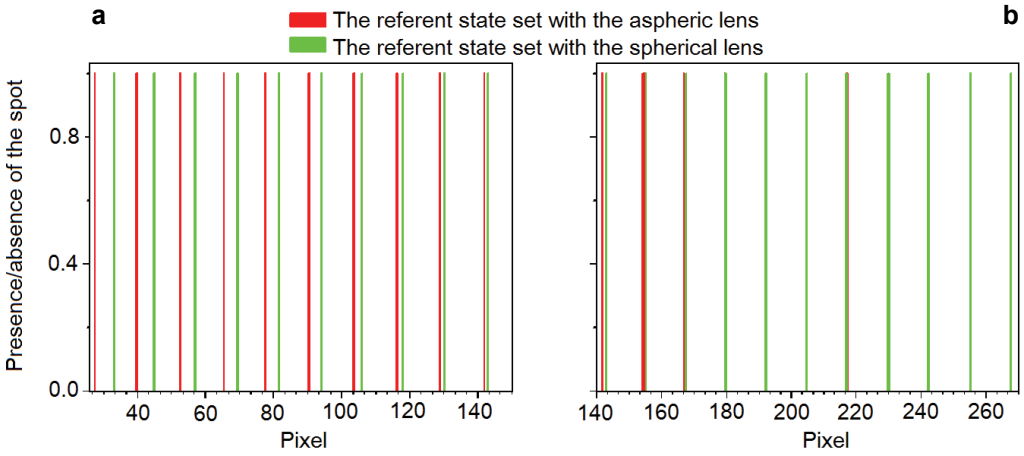

Fig. 3. Reference spot positions obtained by using the spherical (green bars) and the aspheric (red bars) collimating lens. Panel (**a**) shows the peripheral region of the lens while panel (**b**) shows the central region. Spot positions have been calculated by centroiding algorithms. In the center of the spot pattern (around pixel coordinate 260) spot positions in both cases overlap whereas towards the periphery the sphericity of the spherical lens causes the reference positions to deviate away.

determined by calculating the maximal curvature of the wavefront incident on the lenslet array, so that the peripheral spots do not enter the neighbouring region. The area of each lenslet extends halfway the distance between two lenslets, *i.e.*, 75 μm. The local slope can be calculated according to the equations [5]:

$$\frac{\partial W(x,y)}{\partial x} = \frac{\Delta x_s}{F}$$
$$\frac{\partial W(x,y)}{\partial y} = \frac{\Delta y_s}{F} \tag{4}$$

where the Δx_s and Δy_s are the displacements of the centroids, and F is the focal length of the lenslets. In the SHWS model, we use (SHAH-0620A) $F = 3$ mm = 3000 μm. By calculating the slope and the curvature of the wavefront the dynamic range is determined to be about 8 D which is a value comparable to the large dynamic range 10 D of the SHWS used by YOON *et al*. [13] for measuring highly aberrated eyes.

It can be seen in Figures 3**a** and 3**b** that in the central regions centroids calculated for the spherical and the aspheric reference coincide with each other, whereas in a far peripheral region of the pixel array the centroids have been displaced by 4.9 pixels equal to $4.9P = 57.58$ μm because of the spherical aberration. From Eq. (4) the slope and the radius of curvature of the wavefront incident on the lenslet array $R \approx 0.163$ m can be calculated. This corresponds to the optical power +6.1 D.

The spherical aberration of the lens was calculated by using freely available OSLO software intended for various simulation tasks in optics. The entrance pupil of the SHWS is 36 mm and that is why we calculated the longitudinal spherical aberration at a distance of 18 mm from the optic axis. By choosing the appropriate values of curvature of the surfaces, the focal length and the diameter of the lens, the value of the longitudinal spherical aberration of 3 mm was obtained. This corresponds to a change in optical power 0.15 D when compared to the paraxial region.

Relay lenses with the focal length 240 mm and 40 mm and magnification $M = 6$ are placed in front of the lenslet array. The curvature of the wavefront incident on the lenslet array is calculated by using the basic lens equation

$$\frac{1}{l'} = \frac{1}{l} + F \tag{5}$$

where l' is the distance of the image from the lens, l is the distance of the object from the lens, but F is the optical power of the lens.

The spherical lens was placed about 200 mm away from the entrance pupil of the SHWS. Thus the object for the first relay lens with the focal length $f = 240$ mm was placed about 5.8 m behind the lens. By using the lens equation (5) it can be calculated that the image formed by the first relay lens is located about 230.4 behind this lens, *i.e.*, about 49.5 mm before the second relay lens with the focal length $f = 40$ mm. Now, by applying the lens equation (5) again it can be calculated that

the curvature of the wavefront incident on the lenslet array is about 207 mm corresponding to the optical power +4.82 D. This is close to the value calculated from the displacements of the centroids. Thus we conclude that 0.15 D is a reasonable estimate of the spherical aberration of the lens used for setting the reference state.

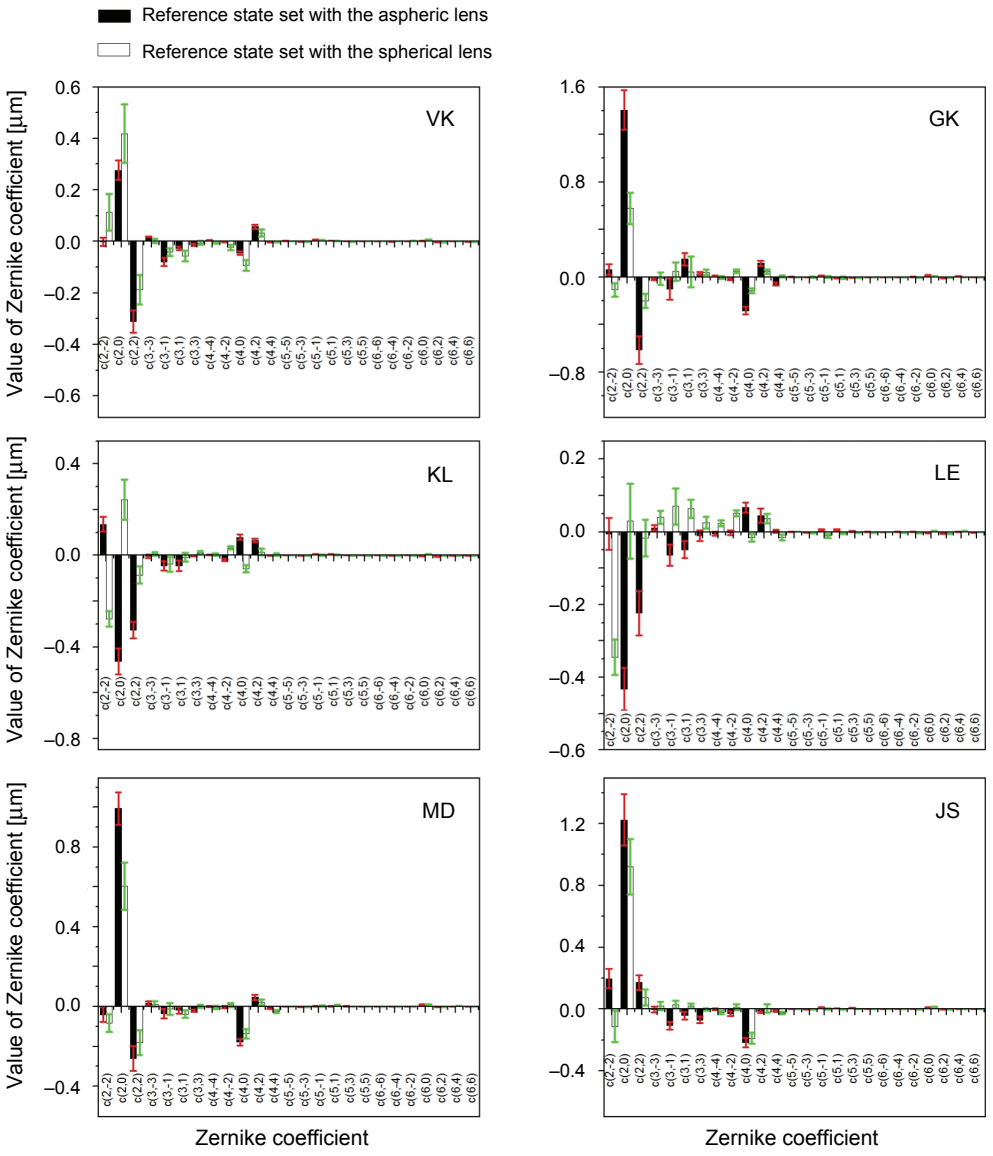

Fig. 4. Measured Zernike coefficients for all the subjects (identified by the initials) and measured against both references. Black columns show aberrations measured against the aspheric reference, white columns are shown for the spherical reference. Piston and tip/tilt are excluded. Zernike coefficients up to the 6th order have been shown. The error bars shown are standard errors calculated from 5 measurements.

3.2. Measurements of aberrations

Next, results of the measurements of ocular aberrations are given. The measured Zernike coefficients for each subject are shown in Fig. 4. Piston and tip/tilt are excluded since these aberrations do not change the shape of the wavefront. Zernike coefficients up to the 6th order have been shown.

As expected, the LOA had the largest magnitude and also demonstrated the largest dependence on the type of the reference. Among HOA spherical aberration c_4^0 had the largest magnitude measured against either reference. In Table 2 the total RMS, the LOA RMS and the HOA RMS have been summarized for each subject. Among HOA the magnitude of coma and spherical aberration was influenced most by the type of the reference state.

In general, both the total RMS and LOA RMS, and HOA RMS were smaller when measured against the spherical reference compared to the aspheric reference. LOA contributed most to reduction of total RMS when measuring aberrations against the spherical reference. HOA RMS changed by only some hundredths of μm.

Table 3 shows the calculated power vectors for both the aspheric and the spherical reference.

T a b l e 2. The total RMS, LOA RMS, and HOA RMS in the case of the aspheric and the spherical reference.

	Total RMS [μm]		LOA RMS [μm]		HOA RMS [μm]		Pupil size
Subject	Asph	Sph	Asph	Sph	Asph	Sph	[mm]
VK	0.431	0.488	0.415	0.472	0.114	0.123	5.5
GK	1.578	0.601	1.536	0.522	0.363	0.299	5.2
KL	0.596	0.387	0.583	0.290	0.123	0.080	5.2
JS	1.279	0.952	1.252	0.931	0.258	0.196	4.5
LE	0.501	0.369	0.487	0.346	0.115	0.128	4.7
MD	1.045	0.652	1.028	0.635	0.190	0.148	4.7

T a b l e 3. Power vectors calculated from Zernike coefficients for both the aspheric and the spherical reference.

	Refractive error predicted by Eq. (3)				
	Sphere	Cylinder $\left(\sqrt{J_{45}^2 + J_0^2}\right)$	Sphere	Cylinder $\left(\sqrt{J_{45}^2 + J_0^2}\right)$	
Subject	Aspheric reference		Spherical reference		Pupil size [mm]
VK	–0.48	+0.41	–0.85	+0.29	5.5
GK	–2.71	+0.83	–1.12	+0.38	5.2
KL	+0.83	+0.48	–0.51	+0.32	5.2
JS	–3.02	+0.39	–2.45	+0.16	4.5
LE	+0.92	+0.39	–0.14	+0.55	4.7
MD	–2.28	+0.43	–1.57	+0.26	4.7

4. Discussion

First, we discuss validity of the wavefront data in the case of the aspheric reference. LOA dominated among all ocular aberrations as expected. The subjects LE and KL had a low degree of hypermetropia while the subject VK had a low degree of myopia, as shown in Tab. 1. The LE, KL, and VK subjects refractive data corresponded well with the power vectors M, J_0, and J_{45} calculated from Eqs. (3) (see Tabs. 1 and 3 for comparison). Equations (3) gave reasonable results only when expanded to include secondary spherical aberration c_6^0. In order to obtain a still better estimate of objective refraction from the wavefront data other Zernike coefficients should be included. However, no direct simple relationship exists between the power vectors and higher Zernike coefficients [14]. Among HOA measured spherical aberration dominated over all other aberration types. In subjects KL and LE small positive spherical aberration was observed whereas small negative spherical aberration was observed in subject VK. The amount and sign of spherical aberration in subjects LE, KL, and VK is in accordance with results of studies investigating development of ocular aberrations with age. Positive spherical aberration is observed in emmetropic and hypermetropic subjects as noted by MARTINEZ *et al*. [15] and increases also with age. Myopic subjects tend to have negative spherical aberration [16].

Subjects GK, JS, and MD had a myopic refractive error, as shown in Table 1. In addition, the subject GK's refractive error was classified as high. While calculated power vectors corresponded well with the actual refractive error for subjects JS and MD there was a discrepancy observable for subject GK (see Tabs. 1 and 2 for comparison). The discrepancy may result from large spot deviations and assignment to the incorrect lenslets as noted by LUNDSTRÖM and UNSBO [17], *i.e.*, the wrapping effect which is likely to occur in our SHWS model because it has a relatively short focal length of the lenslets (f = 3 mm) and small lenslet pitch (150 μm). From the column diagrams in Fig. 3**a** it can be seen that the peripheral spots enter the area of the neighbouring lenslets. As regards spherical aberration the three subjects demonstrated negative spherical aberration which may seem contrary to what is to be expected, *i.e.*, spherical aberration becomes positive with age [18–20]. However, there are studies confirming that in the case of a myopic error spherical aberration may become negative [16, 21].

Next, we analyze the wavefront aberrations measured against the spherical reference. As previously, LOA had the largest magnitude among all aberrations and spherical aberration dominated among HOA. In general, both the total RMS and LOA RMS, and HOA RMS were smaller when measured against the spherical reference compared to the aspheric reference. In subjects KL and LE an increase in defocus c_2^0 was accompanied by reduction in spherical aberration. Reduction in spherical aberration can be attributed to the presence of spherical aberration in the reference, *i.e.*, it is cancelled out. In subject VK defocus increased whereas spherical aberration decreased. Subjects with high degree of myopia (GK, JS, MD) also demonstrated the reduction in the measured spherical refractive error. Power vectors calculated from

Zernike coefficients measured against the spherical reference are summarized in Tab. 2. It can be concluded that small degree of myopia/hypermetropia may be missed and the other type of ametropia may be measured instead. Moderate levels of myopia (like in subjects JS and MD) are underestimated. The discrepancy between power vectors and the refractive data for the subject GK is still larger than in the case of the aspheric reference. It can be concluded that the use of a spherical reference limits the dynamic range of a SHWS similarly to the wrapping effect and these effects sum up.

The results show that measured aberrations vary with the reference against which these aberrations are measured. The reason of variations is spherical aberration of the lens L2 (see Fig. 1). The effect is even more enhanced by the relay lenses with magnification $M = 6$ placed in front of the lenslet array. As could be expected larger variations were observed in the magnitude of LOA although magnitude of HOA was also different in both cases. Many researchers have studied distribution of Zernike terms in large populations. Not only the magnitude of ocular aberrations differs when measured by different aberrometry methods [22, 23] but also there are variations in wavefront data between different SHWS [10]. VISSER *et al*. compared four commercial wavefront aberrometers, two of which (Irx3 and Keratron) were based on Shack–Hartmann principle. The measurements were performed for pupil size 5 mm. The dioptric difference in defocus c_2^0 between Irx3 and Keratron was about 1 D corresponding to 0.92 μm RMS difference for c_2^0 in the case of a 5 mm pupil. This difference is clinically significant. Significant changes in magnitude of spherical aberration and trefoil were observed as well. We suggest that this difference may arise from differences in calibration procedure of both instruments.

DOBOS *et al*. [23] compared refractive error by using both an autorefractometer and also a Bausch & Lomb Zywave aberrometer. For a 5 mm pupil the difference between defocus values measured by both methods was as large as 0.3 D. This corresponds to coefficient c_2^0 difference of approximately 0.3 μm. LIANG *et al*. [24] compared HOA measured by three aberrometers (WaveScan, LADARWave, and ZyWave) based on working principle of a SHWS. What they observed is that HOA RMS could differ by as much as 0.2 μm between different aberrometers. This again raises the question about the origin of these differences.

PLAINIS and PALLIKARIS [25] measured ocular aberrations up to the 6th order in a large emmetropic population by using an Allegretto wavefront analyzer. They reported as small magnitude of spherical aberration as 0.08 μm over a 6 mm pupil. However, other studies report much higher magnitude of spherical aberration [26, 27]. They concluded that the SHWS had internal positive spherical aberration that was partially compensated by the negative spherical aberration in young eyes. We suppose that our SHWS model had some internal positive spherical aberration like Allegretto wavefront analyzer did.

The significance of these changes in magnitude of ocular aberrations can be analyzed from the clinical point of view. The choice of the reference is essential whenever assessing the magnitude of ocular aberrations and inspecting optical quality of an eye. Precise assessment of optical quality is needed also when evaluating

aberrations in keratoconic eyes [28, 29], performance of intraocular lenses [30], effectiveness of refractive surgery [31, 32], *etc*.

We observed changes in magnitude of spherical aberration depending on which reference was used. Spherical aberration is known to influence contrast sensitivity, visual acuity, depth-of-focus and other visual functions [15, 18]. MESTER *et al*. [33] compared Z9000 intraocular lens to SI-40 intraocular lens. The latter had significant amount of spherical aberration contrary to Z9000 which was free of spherical aberration. Implantation of the Z9000 IOL showed apparent improvement in low-contrast visual acuity and contrast sensitivity compared to SI-40.

ROCHA *et al*. [30] compared three different IOLs (AcrySof IQ, AcrySof SN60AT, Sensar AR40) by measuring the depth-of-focus. AcrySof IQ had almost no spherical aberration while AcrySof SN60AT had 0.24 μm spherical aberration. Except for considerable amount of spherical aberration, the latter showed significantly better depth-of-focus when compared to the IOL that was free of spherical aberration. We conclude these studies clearly indicate that precise assessment of spherical aberration of IOL is essential in predicting visual performance and the choice of the reference state is thus essential.

Different laser surgery methods (*e.g.*, LASIK and LASEK) are often compared by measuring the amount of different aberrations postoperatively. MCALINDEN compared changes in ocular aberrations after LASIK and LASEK surgery by using OPD-Scan II (NIDEK Co. Ltd., Gamagori, Japan). The differences between changes in the amount of HOA were only some hundredths. However, there are studies each of which investigates the amount of HOA after LASIK or LASEK and each uses a different wavefront sensor [34, 35]. As can be concluded from our results differences in calibration procedure may result in changes of the amount of HOA larger than few hundredths. Therefore, we conclude that both surgery techniques may be directly compared only given that one and the same aberrometer is used like MCALINDEN did.

The presence of spherical aberration in the reference may result in improper correction of ocular spherical aberration by adaptive optics. If it is assumed that the precise values of Zernike coefficients are those measured in the case of an aspheric reference, then in the case of using a spherical reference there may be some residual amount of spherical aberration after adaptive optics correction. The magnitude of spherical aberration c_4^0 in both cases could differ by as much as 0.2 μm. It has been shown that the magnitude of spherical aberration 0.1 μm can influence contrast sensitivity. PÉREZ *et al*. [18] investigated an impact of scattering and spherical aberration on contrast sensitivity. PÉREZ *et al*. performed visual tests in the presence of controlled amounts of defocus, spherical aberration and scattering. The authors came to an interesting conclusion, *i.e.*, when intraocular scattering is present in the eye the degrading effect of spherical aberration on contrast sensitivity is diminished. However, this was not true for scatter-free eyes.

PIERS *et al*. [32] investigated the optimal magnitude of ocular spherical aberration. They tested the following values: −0.09 μm, 0 μm, 0.09 μm, 0.182 μm. Contrast sensitivity peaked at zero level of spherical aberration. However, the tested values of

spherical aberration are small and possible calibration error should also be included in interpreting the data.

5. Conclusions

For precise measurement of ocular aberrations it is recommended to use the reference set by using either an aspheric lens or an end of a single-mode fibre far away from the entrance pupil of the SHWS.

A possible source of differences between the magnitudes of the aberrations measured by different SHWS is the various radii of curvature of the wavefront used for calibrating the SHWS.

Acknowledgements – The authors are thankful to the European Social Fund project "Support of doctoral studies at the University of Latvia", Project No. 1DP/1.1.2.1.2./09/IPIA/VIAA/004.

References

[1] YOON G., JEONG T.M., COX I.G., WILLIAMS D.R., *Vision improvement by correcting higher-order aberrations with phase plates in normal eyes*, Journal of Refractive Surgery **20**, 2004, pp. 523–527.

[2] MARCOS S., SAWIDES L., GAMBRA E., DORRONSORO C., *Influence of adaptive-optics ocular aberration correction on visual acuity at different luminances and contrast polarities*, Journal of Vision **8**(13), 2008, pp. 1–12, (article 1).

[3] JUNZHONG LIANG, WILLIAMS D.R., MILLER D.T., *Supernormal vision and high-resolution retinal imaging through adaptive optics*, Journal of Optical Society of America A **14**(11), 1997, pp. 2884–2892.

[4] FERNÁNDEZ J.E., IGLESIAS I., ARTAL P., *Closed-loop adaptive optics in the human eye*, Optics Letters **26**(10), 2001, pp. 746–748.

[5] SEIFERT L., LIESENER J., TIZIANI H.J., *The adaptive Shack–Hartmann sensor*, Optics Communications **216**(4–6), 2003, pp. 313–319.

[6] JINGYUN WANG, CANDY T.R., *Higher order monochromatic aberrations of the human infant eye*, Journal of Vision **5**(6), 2005, pp. 543–555, (article 6).

[7] CHERNYSHOV A., STERR U., RIEHLE F., HELMCKE J., PFUND J., *Calibration of a Shack–Hartmann sensor for absolute measurements of wavefronts*, Applied Optics **44**(30), 2005, pp. 6419–6425.

[8] ARTZNER G., *On the absolute calibration of Shack–Hartmann sensors and UV laboratory wavefront measurements*, Pure and Applied Optics **3**(2), 1994, pp. 121–132.

[9] MCALINDEN C., MOORE J.E., *The change in internal aberrations following myopic corneal laser refractive surgery*, Graefe's Archive for Clinical and Experimental Ophthalmology **249**(5), 2011, pp. 775–781.

[10] VISSER N., BERENDSCHOT T.T.J.M., VERBAKEL F., TAN A.N., DE BRABANDER J., NUIJTS R.M.M.A., *Evaluation of the comparability and repeatability of four wavefront aberrometers*, Investigative Ophthalmology and Visual Science **52**(3), 2011, pp. 1302–1311.

[11] XIAOMING Y., XIANG L., LIPING Z., ZHONGPING FANG, *Adaptive thresholding and dynamic windowing method for automatic centroid detection of digital Shack–Hartmann wavefront sensor*, Applied Optics **48**(32), 2009, pp. 6088–6098.

[12] THIBOS L.N., HONG X., BRADLEY A., APPLEGATE R.A., *Accuracy and precision of objective refraction from wavefront aberrations*, Journal of Vision **4**(4), 2004, pp. 329–351.

[13] GEUNYOUNG YOON, PANTANELLI S., NAGY L.J., *Large-dynamic-range Shack–Hartmann wavefront sensor for highly aberrated eyes*, Journal of Biomedical Optics **11**(3), 2006, article 030502.

[14] NAVARRO R., *Objective refraction from aberrometry: Theory*, Journal of Biomedical Optics **14**(2), 2009, article 024021.

[15] MARTINEZ A.A., SANKARIDURG P.R., NADUVILATH T.J., MITCHELL P., *Monochromatic aberrations in hyperopic and emmetropic children*, Journal of Vision **9**(1), 2009, pp. 1–14.
[16] KARIMIAN F., FEIZI S., DOOZANDE A., *Higher-order aberrations in myopic eyes*, Journal of Ophthalmic and Vision Research **5**(1), 2010, pp. 3–9.
[17] LUNDSTRÖM L., UNSBO P., *Unwrapping Hartmann–Shack images from highly aberrated eyes using an iterative B-spline based extrapolation method*, Optometry and Vision Science **81**(5), 2004, pp. 383–388.
[18] PÉREZ G.M., MANZANERA S., ARTAL P., *Impact of scattering and spherical aberration in contrast sensitivity*, Journal of Vision **9**(3), 2009, pp. 1–10.
[19] MOSHIRFAR M., *Spherical aberration of intraocular lenses*, Journal of Ophthalmic and Vision Research **5**(4), 2010, pp. 215–216.
[20] KHAN S., ROCHA G., *Cataract surgery and optimal spherical aberration: As simple as you think?*, Canadian Journal of Ophthalmology **43**(6), 2008, pp. 693–701.
[21] GEUNYOUNG YOON, MACRAE S., WILLIAMS D.R., COX I.G., *Causes of spherical aberration induced by laser refractive surgery*, Journal of Cataract and Refractive Surgery **31**(1), 2005, pp. 127–135.
[22] MCALINDEN C., MOORE J.E., *Higher order aberrations using the NIDEK OPD-Scan and AMO WaveScan*, Journal of Refractive Surgery **26**(8), 2010, pp. 605–608.
[23] DOBOS M.J., TWA M.D., BULLIMORE M.A., *An evaluation of the Bausch & Lomb Zywave aberrometer*, Clinical and Experimental Optometry **92**(3), 2009, pp. 238–245.
[24] CHUNG-LING LIANG, SUH-HANG HANK JUO, CHENG-JONG CHANG, *Comparison of higher-order wavefront aberrations with 3 aberrometers*, Journal of Cataract and Refractive Surgery **31**(11), 2005, pp. 2153–2156.
[25] PLAINIS S., PALLIKARIS I.G., *Ocular monochromatic aberration statistics in a large emmetropic population*, Journal of Modern Optics **55**(4–5), 2008, pp. 759–772.
[26] JINHUA BAO, RONGRONG LE, JIANGXIU WU, YEYU SHEN, FAN LU, JI C. HE, *Higher-order wavefront aberrations for populations of young emmetropes and myopes*, Journal of Optometry **2**(1), 2009, pp. 51–58.
[27] CASTEJÓN-MOCHÓN J.F., LÓPEZ-GIL N., BENITO A., ARTAL P., *Ocular wave-front aberration statistics in a normal young population*, Vision Research **42**(13), 2002, pp. 1611–1617.
[28] RADHAKRISHNAN H., JINABHAI A., O'DONNELL C., *Dynamics of ocular aberrations in keratoconus*, Clinical and Experimental Optometry **93**(3), 2010, pp. 164–174.
[29] KOSAKI R., MAEDA N., BESSHO K., HORI Y., NISHIDA K., SUZAKI A., HIROHARA Y., MIHASHI T., FUJIKADO T., TANO Y., *Magnitude and orientation of Zernike terms in patients with keratoconus*, Investigative Ophthalmology and Visual Science **48**(7), 2007, pp. 3062–3068.
[30] ROCHA K.M., SORIANO E.S., CHAMON W., CHALITA M.R., NOSÉ W., *Spherical aberration and depth of focus in eyes implanted with aspheric and spherical intraocular lenses: A prospective randomized study*, Ophthalmolgy **114**(11), 2007, pp. 2050–2054.
[31] MCALINDEN C., MOORE J.E., *Comparison of higher order aberrations after LASIK and LASEK for myopia*, Journal of Refractive Surgery **26**(1), 2010, pp. 45–51.
[32] PIERS P.A., MANZANERA S., PRIETO P.M., GORCEIX N., ARTAL P., *Use of adaptive optics to determine the optimal ocular spherical aberration*, Journal of Refractive Surgery **33**, 2007, pp. 1721–1726.
[33] MESTER U., DILLINGER P., ANTERIST N., *Impact of a modified optic design on visual function: Clinical comparative study*, Journal of Cataract and Refractive Surgery **29**(4), 2003, pp. 652–660.
[34] CHI-XIN DU, YE SHEN, YANG WANG, *Comparison of high order aberration after conventional and customized ablation in myopic LASIK in different eyes of the same patient*, Journal of Zhejiang University – Science B **8**(3), 2007, pp. 177–180.
[35] URGANCIOGLU B., BILGIHAN K., OZTURK S., *Higher-order aberrations and visual acuity after LASEK*, International Ophthalmology **28**(4), 2008, pp. 269–273.

Received September 16, 2011